Computer Aided Modeling of HgCdTe based Photodetector for NO_2 Gas Detection

Trilok Kumar Parashar,
University Polytechnic, Birla Institute of Technology, MESRA, Ranchi
Email: parashar303017@rediffmail.com

ABSTRACT

In this work an analytical modelling of highly doped p^+-$Hg_{0.73}Cd_{0.27}Te$ over lightly doped n-$Hg_{0.73}Cd_{0.27}Te$ homojunction Photodetector has been analysed theoretically at 77K. A generic model of HgCdTe based on photovoltaic detector has been developed using the closed form equations. Device parameters are obtained by the proposed Photodetector and studied in terms of dark current, resistance area-product, quantum efficiency and detectivity. This high detectivity is 4.9×10^8 $mHz^{1/2}/W$ and efficiency is obtained in the basis of the model lies in wavelength range 7 µm - 9µm with their peaks at about 7.8 µm wavelength, which reveals that this detector is best suited for detection of gas such as NO_2 (7.8 µm).

KEYWORDS: *Modelling, Detectivity, Efficiency, Gas detector;*

1. INTRODUCTION

In this Paper, the Photodetectors based on HgCdTe will be discussed.The ternary alloy $Hg_{1-x}Cd_xTe$ has become an important candidate for optoelectronic devices and optical gas sensor applications because it has wide band-gap range, better stability and it also has weak dependence of the energy gap bandwidth on composition. No single known material surpasses MCT in fundamental performance and flexibility. Photovoltaic detectors fabricated from HgCdTe offers fast response time, higher sensitivity and/or higher operating temperatures over other infrared detectors .Over the past few years, there has been tremendous progress in the development of HgCdTe based infrared photovoltaic detectors due to growing demand for both civilian (earth observation, environment sensing and monitoring) and military (target discrimination and identification, background clutter rejection) applications. Mercury Cadmium Telluride(MCT) detectors have been the most important semiconductor for mid to very long-wavelength (3-30 µm) infrared Photodetectors. One major of utilization of these detector are in gas sensors in infrared region. A number of pollutant combustible/toxic gases and liquids such as hydrocarbons, Ammonia, Sulfur Dioxide, Nitrogen Dioxide, Nitric Oxide, Carbon Monoxide, Hydrogen Sulfide, Hydrogen Cyanide, Hydrogen Chloride, Chlorine, Arsine, Chlorine Dioxide, Fluorine, Hydrogen, Hydrogen Fluoride etc. having their characteristic absorption band located in the infrared region. One basic drawback of these HgCdTe based devices are that they need to be operated in 77K temperature. But in compared to the ease of developed processing technology and remarkable performance obtained, it can be ignored[1]-[9].

2. STRUCTURE

Structure consists of highly doped p^+-$Hg_{0.73}Cd_{0.27}Te$ over lightly doped n-$Hg_{0.73}Cd_{0.27}Te$ shown in Fig.1. which is virtually grown on CdZnTe which is one of the best suitable substrate for HgCdTe detectors. The light has been assumed to be incident on the top p^+- $Hg_{0.73}Cd_{0.27}Te$ side of the Photodetector to collect large quantity of illumination.

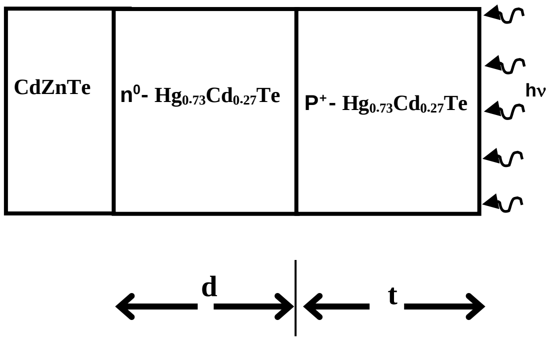

Fig.1. Structure of the Photodetector

3. ANALYTICAL MODELING

Numerical computations have been carried out on p^+-$Hg_{0.73}Cd_{0.27}Te$/ n- $Hg_{0.73}Cd_{0.27}Te$/ CdZnT p^+n homojunction Photodetector at 77K for operation at LWIR. The light has been assumed to be incident on the top p^+- $Hg_{0.73}Cd_{0.27}Te$ side of the Photodetector. The photons with energy higher than the energy gap create electron-hole pairs in p and n region. The band gap of $Hg_{1-x}Cd_xTe$ as a function of temperature T and alloy composition x is included in the simulation model using the empirical formula [1-2].

Dark Current

The major components of dark current in p^+-$Hg_{0.73}Cd_{0.27}Te$/ n- $Hg_{0.73}Cd_{0.27}Te$/ CdZnT homojunction PIN-Photodetector include (i) the diffusion of the thermally generated carriers from the neutral regions, I_{DIFF} (ii) generation-recombination of carriers in the depletion region, I_{GR} (iii) tunneling of carriers through the barrier, $I_{TUN.}$ In order to generalize the analysis, we have however considered both trap assisted tunneling (TAT) as well as band-to-band tunneling (BTB). The tunneling component of current thus constitutes two components e.g., I_{TAT} arising from the trap assisted tunneling and I_{BTB} arising out of band-to-band tunneling. The net the top p+ layer receives the incident light through CdZnTe substrate, which is transparent to incident light, and the lightly doped n^0 region acts as the active layer. The incident light is absorbed in the neutral p^+, n^0 regions as well as in the space charge region formed at the p^+-n^0 junction. The interfacial surface recombination due to non-ideal passivation conditions has also been considered in present model. The magnitude of total dark current of the Photodetector is [1]

$$I_{net} = I_{diff} + I_{gr} + I_{tat} + I_{btb} \quad [1]$$

The product of dynamic resistance and area (R_0A) is given by the reciprocal of the derivative of the current density with respect to the voltage.

$$\frac{1}{(R0A)} = \frac{dJ}{dV} \quad [2]$$

Quantum Efficiency

The quantum efficiency (η) of a p-n junction Photodetector has generally three major components. These components arise from the contribution of the three regions e.g., neutral n-region (η_n), neutral the optical generation p-region (η_p) and the depletion region (η_{dep}) rate of electron-hole pairs, as a function of distance x from the surface can be written as [1]

$$\eta = \eta_n + \eta_p + \eta_{dep} \quad [3]$$

Specific Detectivity

The most important figure of merit of the Photodetector for use toxic gas monitoring is the specific detectivity D^*, which depends on the wavelength of incident light λ, the quantum efficiency η and zero bias resistance area product (R_0A) [1].

$$D^* = \frac{q\eta\lambda}{hc}\sqrt{\frac{R_0 A_{net}}{4kT}} \quad [4]$$

Responsivity

The responsivity ($\Re$) of the Photodetector depends on the wavelength of incident light λ, the quantum efficiency η [1]. The equation to obtain responsivity is given as

$$\Re = \frac{\eta q \lambda}{hc} \quad [5]$$

4. Results and Discussions

In Fig.2., Shows the variation of the net dark current along with its component due to major three recombination mechanism diffusion, generation-recombination and tunnelling (BTB+TAT) with the applied bias voltage. Just like first problem current flows in the detector due to diffusion. Due to their very small values, the GR and BTB component of dark current could not affect the total dark current considerably.

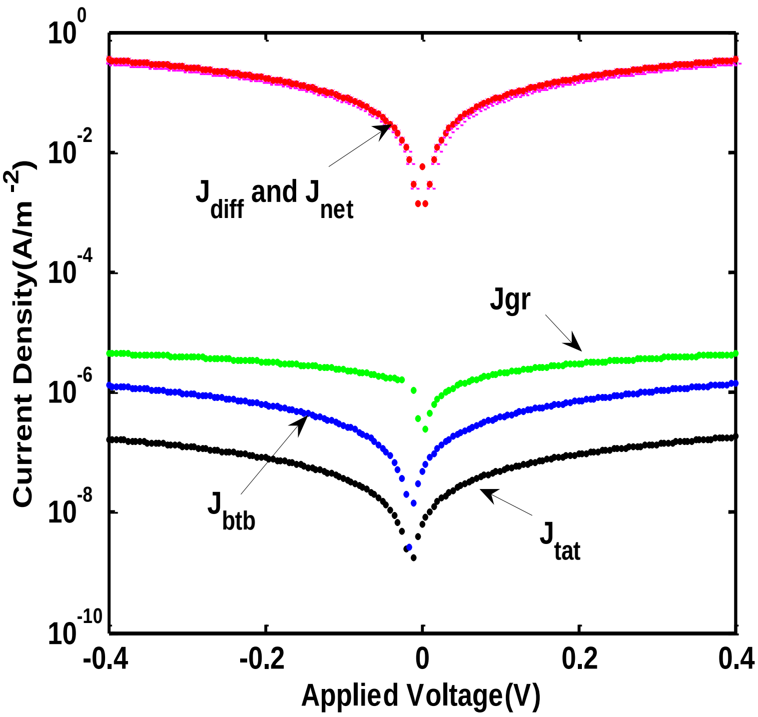

Fig.2. current density and its component with respect to applied voltage

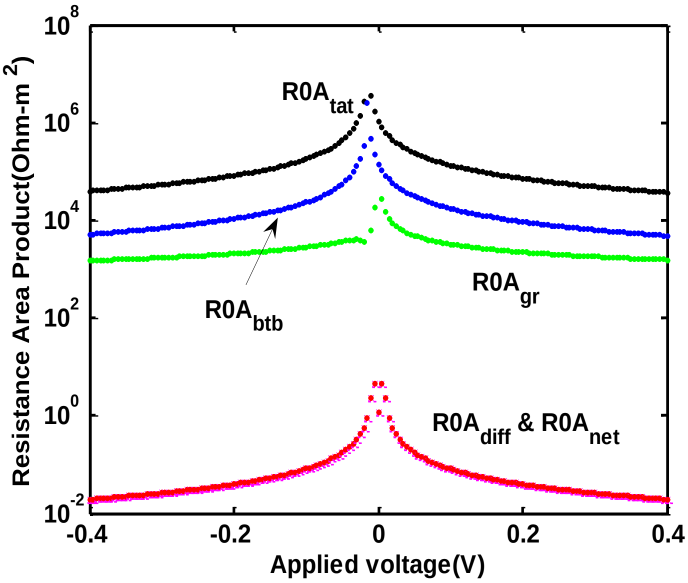

Fig.**3**. R_0A_{net} and its component with respect to applied voltage

In Fig.3., shows the variation of R_0A_{net} along with its component (recombination mechanism diffusion, generation-recombination and tunnelling). It is also clear from figure net zero bias resistance area product dominated by diffusion component. Due to their very small values the GR and BTB component of resistance area product could not affect the net zero bias resistance area product

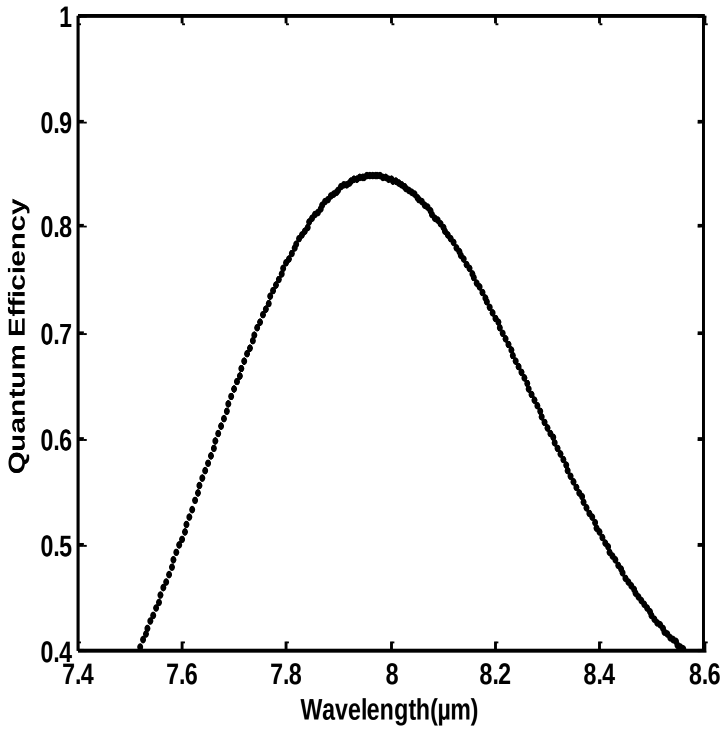

Fig. **4**. Quantum efficiency with respect to operating wavelength

The quantum efficiency and specific device are the two main device parameter in terms of which the performance of the detector is described. Fig.4., shows variation of the efficiency of the detector with respect to operating wavelength has been presented.

In present case, the efficiency of the detector achieves its maximum value ~ 0.8 at 7.8 µm. It decreases sharply on the both side. One can see that the efficiency wavelength ranges 7 µm to 9 µm which may be consider the range over which the device can be utilise as detector.

In Fig 5., variation of the responsivity of the detector with respect to operating wavelength has been presented. Here the peak responsivity 5.5 A/W is obtained at 7.8 µm.

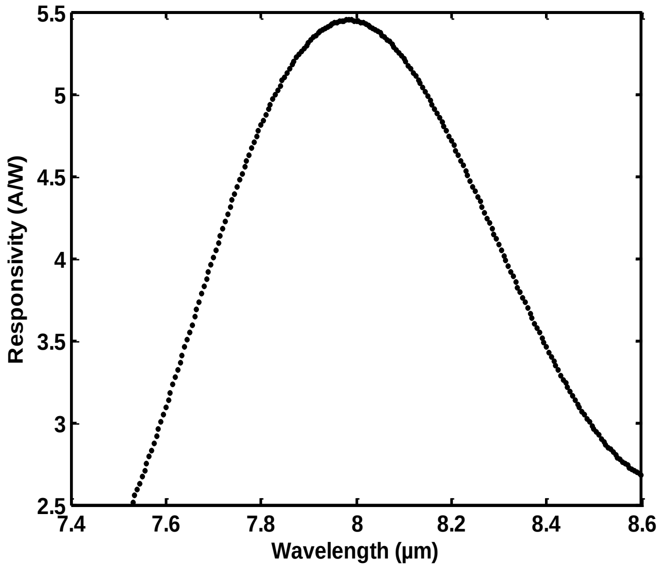

Fig. **5**. Responsivity with respect to operating wavelength

The variation of detectivity with operating wavelength shown in last Fig.6.; here also the peak detectivity (~ 4.9×10^{8}mHz$^{1/2}$/W) is obtained at the wavelength λ~ 7.8 µm. This is the signature wavelength of the nitrous oxide (NO_2) gasis 7.8 µm.

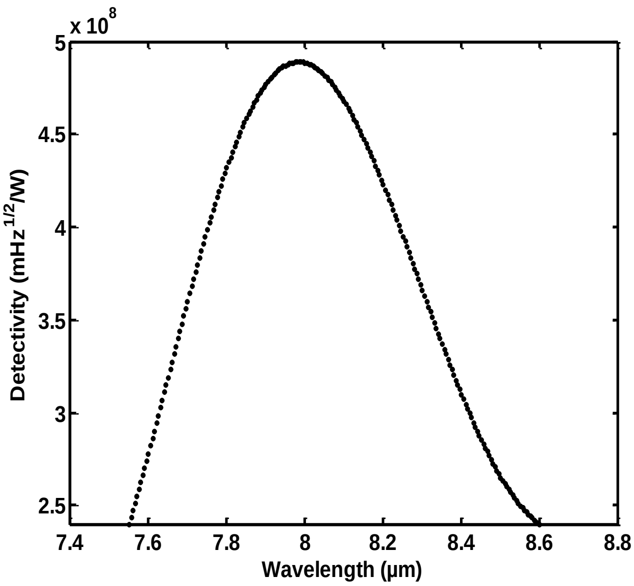

Fig. **6**. Detectivity with respect to operating wavelength

For non-telecommunication applications such as gas sensor device can be utilised as detector for NO_2 gas whose characteristic wavelength is 7.8 µm.

Comparison: The performance parameters of the Photodetector obtained on the basis of our model are found to be in good match with the results already reported by P.K. Saxena in 2011[10] in Infrared Physics and Technology. The quantum efficiency find from our models are better than P. K. Saxena Models. The comparison results are shown in the Table 1.0.

Table 1.0 Comparison Table1.0

Parameter	**Result of our Ist model**	**Result reported by P. K. Saxena 2011[10]**
Structure	p^+-n Homojunction $Hg_{0.73}Cd_{0.27}Te$ detector	p^+-n Homojunction $Hg_{0.88}Cd_{0.22}Te$
J_{Net}	~ 1.0 × 10^{-1}	~5× 10^{-5}A
Dynamic Resistance	~1× 10^{-2}	~2× 10^{4}A
Quantum Efficiency	**0.85**	0.8
Peak Detectivity	**~ 4.9× 10^{8} m$Hz^{1/2}$/W**	9× 10^{9} m$Hz^{1/2}$/W
Cutoff Wavelength	~7.9µm	10.6 µm

5. CONCLUSION

The performance of the HgCdTe Photodetector has been examined by self-generated MATLAB code for Photodetector to compute the dark current density, zero bias area product, quantum efficiency, responsivity and detectivity.
Results of our study in this problem reveal that high detectivity (=4.9×10^{8} m$Hz^{1/2}$/W) and efficiency obtained on the basis of the model lies in wavelength range 7 µm - 9µm with their peaks at about 7.8 µm wavelength, which reveals that this detector is best suited for detection of gases such as NO_2 (7.8 µm), H_2O (7.7 µm), C_2H_2 (7.6 µm).

REFERENCES

[1]. T.K.Parashar and R.K.Lal, "Modeling and Simulation of HgCdTe based Photodetector for N2O gas detection", Journal of Electron Devices, Vol. 11, pp. 527-537, (2011).

[2]. T. K. Parashar and R. K. Lal, "Effect of temperature and mole fraction on carrier lifetime of HgCdTe material", Recent Developments in Engineering Materials (RDEM-2011). Organized by BIT Mesra, Ranchi, ,.ISBN:978-93-82062-21-9. pp-56.11-14 may, (2011).

]3]. A Rogalski, J Antoszewski and L Faraone,"Third-generation infrared Photodetectorarrays," J. Appl. Phys. 105, 09110, (2009).

[4]. Chang Y, Grein C H, Zhao J, Becker C R, Flatte M E, Liao P K, Aqariden F and Sivananthan S. "Carrier recombination lifetime characterization of molecular beam epitaxially grown HgCdTe," Appl. Phys. Lett. 93, 19211, (2008).

[5]. Le Perchec J, Y Desieres and Espiau de R Lamaestre,"Plasmon-based photosensors comprising a very thin semiconducting region," J. Appl. Phys. Lett, 94, 181104, (2009).

[6]. A Zemel, I Lukomsky and J. E Weiss."Mechanism of carrier transport across thejunction of narrow band-gap planar n+p HgCdTe photodiodes grown by liquid-phase epitaxy," J Appl.Phys, 98, 054504,(2005).

[7]. A. Rogalski, K. Adamiec and J. Rutkowski, "Narrow-Gap Semiconductor Photodiode", SPIE Press, Bellingham, USA, (2000).

[8]. A. Rogalski,"Third generation infrared detectors Proceedings of the Symposium on Photonics Technologies for 7th Framework Program, Wroclaw 12-14 October, (2006).

[9]. M Mello, B Poti1, A Risi, A de Passaseo, M Lomascolo and M. De Vittorio, “GaN optical system for CO and NO gas detection in the exhaust manifold of combustion engines,” J. Opt. A: Pure Appl. Opt. 8, S545–S549, (2006).

[10]. P.K., Saxena, “Modeling and simulation of HgCdTe based p+–n–n+ LWIR Photodetector,” Infrared Physics & Technology 54 25–33,(2011).

AUTHORS BIOGRAPHY

Dr. Trilok Kumar Parashar, University Polytechnic, Birla Institute of Technology, MESRA, Ranchi
Email: parashar303017@rediffmail.com
Email: tkparashar@bitmesra.ac.in